

Recent advances in the chemistry of lanthanide-doped upconversion nanocrystals

Feng Wang and Xiaogang Liu*

Received 13th October 2008

First published as an Advance Article on the web 12th February 2009

DOI: 10.1039/b809132n

Lanthanide ions exhibit unique luminescent properties, including the ability to convert near infrared long-wavelength excitation radiation into shorter visible wavelengths through a process known as photon upconversion. In recent years lanthanide-doped upconversion nanocrystals have been developed as a new class of luminescent optical labels that have become promising alternatives to organic fluorophores and quantum dots for applications in biological assays and medical imaging. These techniques offer low autofluorescence background, large anti-Stokes shifts, sharp emission bandwidths, high resistance to photobleaching, and high penetration depth and temporal resolution. Such techniques also show potential for improving the selectivity and sensitivity of conventional methods. They also pave the way for high throughput screening and miniaturization. This *tutorial review* focuses on the recent development of various synthetic approaches and possibilities for chemical tuning of upconversion properties, as well as giving an overview of biological applications of these luminescent nanocrystals.

1. Introduction

Upconversion (UC) refers to nonlinear optical processes characterized by the successive absorption of two or more pump photons *via* intermediate long-lived energy states followed by the emission of the output radiation at a shorter wavelength than the pump wavelength. This general concept was first recognized and formulated independently by Auzel, Ovsyankin, and Feofilov in the mid-1960s.¹ Since then, conversion of infrared radiation into the visible has generated

much of the interest in UC research, progressively generating and incorporating novel areas of investigation. The knowledge gained thus far has allowed the development of some remarkably effective optical devices such as infrared quantum counter detectors, temperature sensors, and compact solid state lasers.

Despite their remarkable potential utility, the practical use of UC has been primarily focused on bulk glass or crystalline materials for the past 30 years but with extremely limited impact on biological sciences. These limitations are largely attributed to the difficulties in preparing small nanocrystals (sub-50 nm) that exhibit high dispersibility and strong UC emission in aqueous solutions. It was not until the late 1990s, when nanocrystal research became prevalent, that UC became more prominent in the fields of biological assays and medical

Department of Chemistry, Faculty of Science, National University of Singapore, 3 Science Drive 3, Singapore 117543.
E-mail: chmlx@nus.edu.sg



Feng Wang

Feng Wang was born on February 16, 1979 in Shaanxi, China. He received his BE (2001) and PhD (2006) degrees in Materials Science and Engineering from Zhejiang University. His PhD thesis was focused on the synthesis and characterization of lanthanide-doped fluoride nanomaterials under the supervision of Profs. Mingquan Wang and Xianping Fan. He joined the group of Prof. Xiaogang Liu at the National University of Singapore in 2007. His current research

focuses on the synthesis, spectroscopic investigation, and application of luminescent nanomaterials.



Xiaogang Liu

Xiaogang Liu was born in Jiangxi, China. He earned his BE degree (1996) in Chemical Engineering from Beijing Technology and Business University. He received his MS degree (1999) in Chemistry from East Carolina University under the direction of Prof. John Sibert and completed his PhD (2004) at Northwestern University under the supervision of Prof. Chad Mirkin. He then became a postdoctoral fellow in the group of Prof. Francesco Stellacci at MIT. He joined the faculty of

the National University of Singapore in 2006. His research interests include nanomaterials synthesis, supramolecular chemistry, and surface science for catalysis, sensors and biomedical applications.

imaging. As high quality UC nanocrystals can now be routinely prepared, the study of these UC processes has evolved into a highly interdisciplinary field that has rapidly expanded at the frontiers of photochemistry, biophysics, solid state physics, and materials science. In particular, UC emission from lanthanide (Ln)-doped nanocrystals offers an attractive optical labeling technique in biological studies without many of the constraints associated with organic fluorophores and quantum dots.^{2,3} The UC technique utilizes near infrared (NIR) excitation rather than ultraviolet (UV) excitation, thereby significantly minimizing background autofluorescence, photobleaching, and photodamage to biological specimens. The technique also allows *in vivo* observation with substantially high spatial resolution and offers remarkable sample penetration depths that are much higher than those obtained by UV excitation.⁴ In addition, UC processes can be induced by a low power ($1\text{--}10^3\text{ W cm}^{-2}$) continuous wave laser, as opposed to a costly high-intensity ($10^6\text{--}10^9\text{ W cm}^{-2}$) pulse laser source for the generation of a simultaneous two-photon process.

UC processes are mainly divided into three broad classes: excited state absorption (ESA), energy transfer upconversion (ETU), and photon avalanche (PA). All these processes involve the sequential absorption of two or more photons (Fig. 1). Thus, UC processes are different from the multiphoton process where the absorption of photons occurs simultaneously.

In the case of ESA, excitation takes the form of successive absorption of pump photons by a single ion. The general energy diagram of the ESA process is shown in Fig. 1a for a simple three-level system. If excitation energy is resonant with the transition from ground level G to excited metastable level E1, phonon absorption occurs and populates E1 from G in a process known as ground state absorption (GSA). A second pump photon that promotes the ion from E1 to higher-lying state E2 results in UC emission, corresponding to the E2 → G optical transition.

ETU is similar to ESA in that both processes utilize sequential absorption of two photons to populate the metastable level. The essential difference between ETU and ESA is that the excitation in ETU is realized through energy transfer between two neighboring ions. In an ETU process,

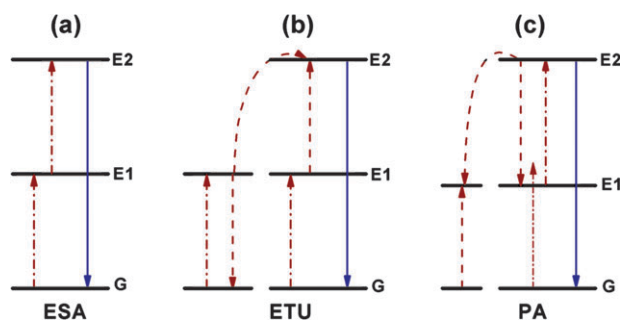


Fig. 1 Principal UC processes for lanthanide-doped crystals: (a) excited state absorption, (b) energy transfer upconversion, (c) photon avalanche. The dashed/dotted, dashed, and full arrows represent photon excitation, energy transfer, and emission processes, respectively.

each of two neighboring ions can absorb a pump phonon of the same energy, thereby populating the metastable level E1 (Fig. 1b). A non-radiative energy transfer process promotes one of the ions to upper emitting state E2 while the other ion relaxes back to ground state G. The dopant concentration that determines the average distance between the neighboring dopant ions has a strong influence on the UC efficiency of an ETU process.

The phenomenon of PA was first discovered by Chivian and co-workers⁵ in Pr^{3+} -based infrared quantum counters. PA-induced UC features an unusual pump mechanism that requires a pump intensity above a certain threshold value. The PA process starts with population of level E1 by non-resonant weak GSA, followed by resonant ESA to populate upper visible-emitting level E2 (Fig. 1c). After the metastable level population is established, cross-relaxation energy transfer (or ion pair relaxation) occurs between the excited ion and a neighboring ground state ion, resulting in both ions occupying the intermediate level E1. The two ions readily populate level E2 to further initiate cross-relaxation and exponentially increase level E2 population by ESA, producing strong UC emission as an avalanche process.

The UC luminescent efficiency in these three processes varies considerably. ESA is the least efficient UC process. Efficient UC is possible in PA with metastable, intermediate levels that can act as a storage reservoir for pump energy. However, the PA process suffers from a number of drawbacks, including pump power dependence and slow response to excitation (up to several seconds) due to numerous looping cycles of ESA and cross-relaxation processes. In contrast, ETU is instant and pump power independent, and thus has been widely used to offer highly efficient UC (\sim two orders of magnitude higher than ESA)¹ over the past decade.

Nanoscale manipulation of lanthanide-doped UC nanocrystals leads to important modification of their optical properties in excited-state dynamics, emission profiles and UC efficiency. For example, the reduction in particle size provides the ability to modify the lifetime of intermediate states.⁶ The control of spatial confinement of dopant ions within a nanoscopic region can lead to marked enhancement of a particular wavelength emission as well as generation of new types of emissions.

This tutorial review focuses primarily on advances developed within the past five years in the rational design and synthesis of lanthanide-doped UC nanocrystals. In section 2, an effort has been made to present an overview of the dopant/host design principle for efficient UC in nanocrystals. In section 3, we discuss a variety of synthetic approaches that offer control over particle size, shape, dispersion, and emission properties. We also provide examples of various systems. In section 4, we attempt to provide general strategies for surface modification of UC nanocrystals, leading to high resistance to quenching induced by solvents or surface defects such as adsorbed contaminants. The surface modification also imparts improved particle dispersibility in the solvent and provides active surfaces for further biological functionalization. In section 5, we provide a general picture of chemical tuning of emission colors, as it emerges from a consideration of the interplay of different parameters that control the emission

process. In section 6, we highlight the emerging applications of these UC nanocrystals in biological sciences.

2. Dopant/host selection criteria

Inorganic crystals in most cases do not exhibit UC luminescence at room temperature. Therefore, research is mainly directed to systems that are composed of a crystalline host and lanthanide dopants added to the host lattice in low concentrations. This is especially important when having in mind the potential preparation of new nanomaterials with well defined optical properties. The dopants are usually in the form of localized luminescent centers. In the case of the sensitized luminescence, the dopant ion radiates upon its excitation to a higher energetic state obtained from the non-radiative transfer of the energy from another dopant ion. The ion that emits the radiation is called an activator, while the donor of the energy is the sensitizer. Although UC can be expected in principle from most lanthanide-doped crystalline host materials, efficient UC only occurs by using a small number of well selected dopant–host combinations.

2.1 Activators

The requirement of multiple metastable levels for UC makes the lanthanides well-suited for this application. The lanthanides, which are associated with the filling of the 4f-shell, commence with the element lanthanum (La) and end with the element lutetium (Lu). They essentially exist in their most stable oxidation state as trivalent ions (Ln^{3+}). The shielding of the 4f electrons of Ln^{3+} by the completed filled 5s² and 5p⁶ sub-shells results in weak electron–phonon coupling that is responsible for important phenomena such as sharp and narrow f–f transition bands. In addition, the f–f transitions are Laporte forbidden, resulting in low transition probabilities and substantially long-lived (up to 0.1 s) excited states.¹ With the exception of La^{3+} , Ce^{3+} , Yb^{3+} , and Lu^{3+} , the lanthanide ions commonly have more than one excited 4f energy level.

As a consequence, UC emission can be theoretically expected for most lanthanide ions. However, to generate practically useful UC emission, the energy difference between each excited level and its lower-lying intermediate level (ground level) should be close enough to facilitate photon absorption and energy transfer steps involved in UC processes. Er^{3+} , Tm^{3+} , and Ho^{3+} typically feature such ladder-like arranged energy levels and are thus frequently used activators (Fig. 2). For example, the energy difference in Er^{3+} ($\sim 10\,350\text{ cm}^{-1}$) between the $^4\text{I}_{11/2}$ and $^4\text{I}_{15/2}$ levels is similar to that ($\sim 10\,370\text{ cm}^{-1}$) between the $^4\text{F}_{7/2}$ and $^4\text{I}_{11/2}$ levels. Thus, the energy levels of $^4\text{I}_{15/2}$, $^4\text{I}_{11/2}$, and $^4\text{F}_{7/2}$ can be used to generate UC emission using $\sim 970\text{ nm}$ excitation. Instead of being directly excited to the $^4\text{F}_{7/2}$ state, Er^{3+} ion in the $^4\text{I}_{11/2}$ state can relax to the $^4\text{I}_{13/2}$ state, followed by excitation to the $^4\text{F}_{9/2}$ state with phonon-assisted energy transfer.

Non-radiative multiphonon relaxation rate between energy levels is another important factor that dictates the population of intermediate and emitting levels and subsequently determines the efficiency of the UC process. The multiphonon relaxation rate constant k_{nr} for 4f levels of lanthanide ions is described as⁷

$$k_{\text{nr}} \propto \exp\left(-\beta \frac{\Delta E}{\hbar\omega_{\text{max}}}\right)$$

where β is an empirical constant of the host, ΔE is the energy gap between the populated level and the next lower-lying energy level of a lanthanide ion, and $\hbar\omega_{\text{max}}$ is the highest-energy vibrational mode of the host lattice. The energy gap law implies that the multiphonon relaxation rate constant decreases exponentially with increasing energy gap. As shown in Fig. 2, Er^{3+} and Tm^{3+} have relatively large energy gaps and thus low probabilities of non-radiative transitions among various excited levels of the ions. In agreement with the energy gap law, the most efficient UC nanocrystals known to date are obtained with Er^{3+} and Tm^{3+} as the activators.

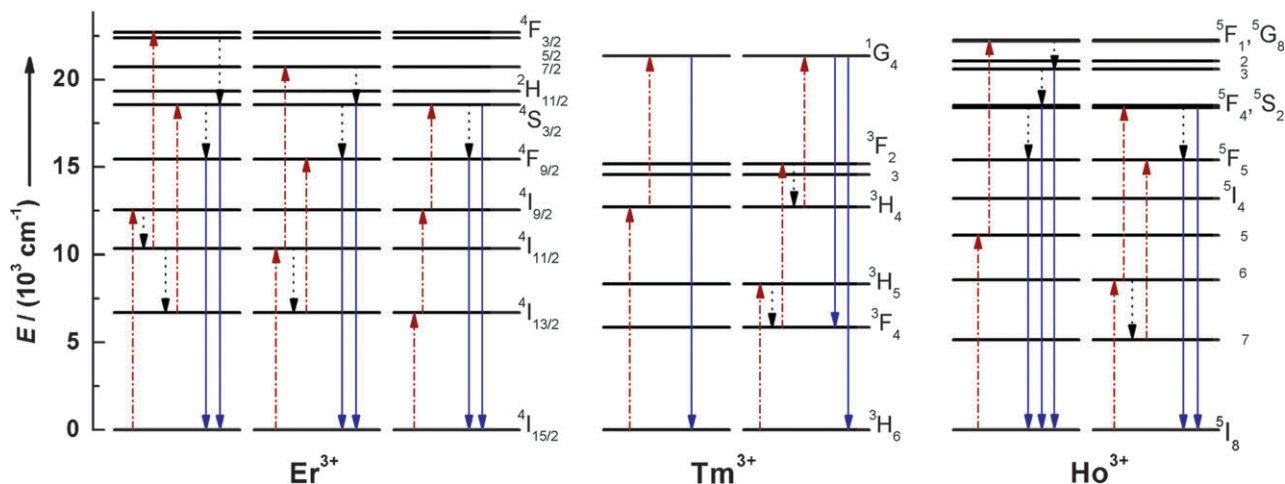


Fig. 2 Schematic energy level diagrams showing typical UC processes for Er^{3+} , Tm^{3+} , and Ho^{3+} . The dashed-dotted, dotted, and full arrows represent excitation, multiphonon relaxation, and emission processes, respectively. The excitation originates from either direct photo excitation or energy transfer. Since energy transfer can occur with the assistance of phonons, the energy differences between each key excited level and its key lower-lying level can be a little inconsistent. The $^{2S+1}L_J$ notations used to label the f levels refer to spin (S), orbital (L) and angular (J) momentum quantum numbers respectively according to the Russel–Saunders notation.

2.2 Sensitizers

In singly doped nanocrystals, the two major parameters that effect UC processes are the distance between two neighboring activator ions and the absorption cross-section of the ions. High doping levels can lead to deleterious cross-relaxation, resulting in quenching of excitation energy. The concentration of activator ions should be kept low and precisely adjusted to avoid the quenching effect. In addition, most lanthanide activator ions exhibit low absorption cross-sections, leading to low pump efficiency. Therefore, the overall UC efficiency for singly doped nanocrystals is relatively low.

To enhance UC luminescence efficiency, a sensitizer with a sufficient absorption cross-section in the NIR region is usually co-doped along with the activator to take advantage of the efficient ETU process between the sensitizer and activator. Trivalent Yb possesses an extremely simple energy level scheme with only one excited 4f level of $^2F_{5/2}$ (Fig. 3). The absorption band of Yb^{3+} that is located around 980 nm due to the $^2F_{7/2} \rightarrow ^2F_{5/2}$ transition has a larger absorption cross-section than that of other lanthanide ions. Additionally, the $^2F_{7/2} \rightarrow ^2F_{5/2}$ transition of Yb^{3+} is well resonant with many f-f transitions of typical upconverting lanthanide ions (Er^{3+} , Tm^{3+} , and Ho^{3+}), thus facilitating efficient energy transfer from Yb^{3+} to other ions. These optical characteristics make Yb^{3+} particularly suitable for use as a UC sensitizer. The sensitizer content is normally kept high (~ 20 mol%) in doubly or triply doped nanocrystals, while the activator content is relatively low (< 2 mol%), minimizing cross-relaxation energy loss.

2.3 Host materials

Selection of appropriate host materials is also essential in the synthesis of lanthanide-doped nanocrystals with favorable

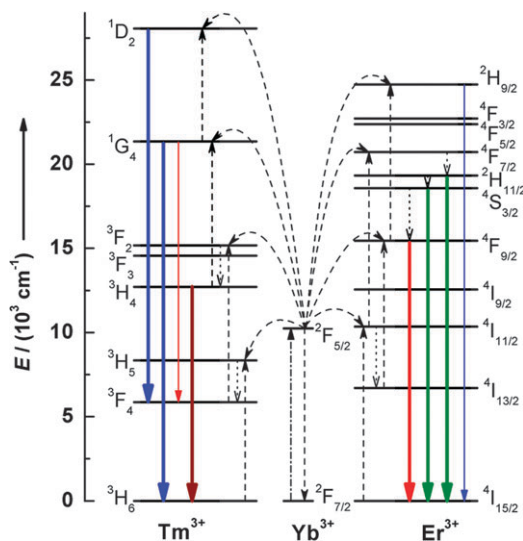


Fig. 3 Proposed energy transfer mechanisms showing the UC processes in Er^{3+} , Tm^{3+} , and Yb^{3+} doped crystals under 980-nm diode laser excitation. The dashed-dotted, dashed, dotted, and full arrows represent photon excitation, energy transfer, multiphonon relaxation, and emission processes, respectively. Only visible and NIR emissions are shown here.

optical properties such as high UC efficiency and controllable emission profile. The host materials generally require close lattice matches to dopant ions and have low phonon energies.

As all trivalent rare earth ions exhibit similar ionic size and chemical properties, their inorganic compounds are ideal host materials for upconverting lanthanide dopant ions. In addition, alkaline earth ions (Ca^{2+} , Sr^{2+} , and Ba^{2+}) and some transition metal ions (Zr^{4+} and Ti^{4+}) also exhibit close ionic size to lanthanide ions. Therefore, inorganic compounds containing these ions are also frequently used as host materials for UC processes. However, lanthanide-doping in these nanocrystals is always accompanied by the formation of crystal defects such as interstitial anions and cation vacancies to maintain charge neutrality. To maintain a single crystal phase of the host for efficient UC, the dopant concentration should be stringently controlled. Semiconductor nanocrystals such as ZnS have also been proposed as UC host materials. However, it is still debatable whether lanthanide ions in these nanocrystals are mainly located on the outermost layer of the nanocrystals due to largely mismatched ionic size between the host and dopant ions or incorporated homogeneously in the host lattice.⁸

Ideal host materials should also have low lattice phonon energies, which is a requirement to minimize non-radiative loss and maximize the radiative emission. Heavy halides like chlorides, bromides and iodides generally exhibit low phonon energies of less than 300 cm^{-1} . However, they are hygroscopic and are of limited use. Oxides exhibit high chemical stability, but their phonon energies are relatively high and generally larger than 500 cm^{-1} due to the stretching vibration of the host lattice. In comparison, fluorides usually exhibit low phonon energies ($\sim 350\text{ cm}^{-1}$) and high chemical stability, and thus are often used as the host materials for UC.

It is also known that the variation of the crystal structure in the host materials can significantly influence the optical properties of nanocrystals. For example, hexagonal-phase $NaYF_4:Yb/Er$ bulk materials exhibit about an order of magnitude enhancement of UC efficiency relative to their cubic phase counterparts.⁹ The phase-dependent optical property can be ascribed directly to the different crystal-fields around trivalent lanthanide ions in matrices of various symmetries. Low symmetry hosts typically exert a crystal-field containing more uneven components around the dopant ions compared to high symmetry counterparts. The uneven components enhance the electronic coupling between 4f energy levels and higher electronic configuration and subsequently increase f-f transition probabilities of the dopant ions.¹⁰ In addition, the decrease in cation size (or unit-cell volume) of the host can cause an increase in the crystal-field strength around the dopant ions and lead to enhanced UC efficiency. For example, the bulk material of $NaYF_4:Yb/Er$ exhibits a UC luminescence two times stronger than that of $NaLaF_4:Yb/Er$.¹⁰

3. Nanocrystal synthesis

A variety of chemical techniques, including coprecipitation, thermal decomposition, hydro(solvo)thermal synthesis, sol-gel processing and combustion synthesis, have been demonstrated to synthesize lanthanide-doped UC nanocrystals (Table 1).

Table 1 Typical synthetic routes to UC nanocrystals

Method	Examples (Hosts)	Remarks
Coprecipitation	LaF ₃ NaYF ₄ LuPO ₄ YbPO ₄	Fast growth rate without the need for costly equipment and complex procedures. Post-heat treatment typically required.
Thermal decomposition	LaF ₃ NaYF ₄ GdOF	Expensive, air-sensitive metal precursors. High quality, monodisperse nanocrystals. Toxic by-products.
Hydro(solvo)thermal synthesis	LaF ₃ NaYF ₄ La ₂ (MoO ₄) ₃ YVO ₄	Cheap raw materials. No post-heat treatment. Excellent control over particle size and shape. Specialized reaction vessels required.
Sol-gel processing	ZrO ₂ TiO ₂ BaTiO ₃ Lu ₃ Ga ₅ O ₁₂ YVO ₄	Cheap raw materials. Calcinations at high temperatures required.
Combustion synthesis	Y ₂ O ₃ Gd ₂ O ₃ La ₂ O ₂ S	Time and energy saving. Considerable particle aggregation.
Flame synthesis	Y ₂ O ₃	Time saving and readily scalable.

Some nanocrystals, especially those with narrow size distribution and high aqueous solubility, require a special method or a combination of several methods, but others can be prepared by many complementary approaches. Optimization of the synthesis or fabrication procedure is critical to obtain nanocrystals with tailored crystal size, morphology, chemical composition, surface functionalization, and optical properties. We focus on some of the most successful approaches to date for synthesizing UC nanocrystals.

Coprecipitation is perhaps one of the most convenient techniques for synthesizing ultrasmall lanthanide-doped nanocrystals with narrow size distribution. Compared to other techniques, there is no need for costly equipment, stringent reaction conditions, and complex procedures, resulting in less time consumption. In some rare instances, crystalline nanoparticles were formed directly by coprecipitation, eliminating the need for a calcination step or post-annealing process. One of the earliest examples of this technique was demonstrated by van Veggel and co-workers,⁶ who made downconversion LaF₃ nanocrystals doped with Ln³⁺ (Ln = Eu, Er, Nd, and Ho). The approach was expanded and refined by Chow and co-workers,¹¹ who synthesized UC LaF₃ nanocrystals with smaller particle size (~5 nm) and narrower size distribution from simple water soluble inorganic precursors (Fig. 4a and b). In their studies, synthetic ammonium di-*n*-octadecylthiophosphate was used as a capping ligand to control particle growth and to stabilize the nanocrystals against aggregation. These sub-10 nm UC crystals can be re-dispersed in solutions, offering promising applications as luminescent probes for biomolecules with dimensions from several nanometres to tens of nanometres. In addition to LaF₃ nanocrystals, NaYF₄:Yb/Er(Tm), LuPO₄:Yb/Tm, and YbPO₄:Er nanocrystals were also synthesized *via* the coprecipitation approach coupled with heat treatment (or post-annealing process) for enhanced UC emission by the groups of Haase, Güdel, Chen, and Li.^{9,12–14} Commercially available ligands such as polyvinylpyrrolidone (PVP) and polyethylenimine (PEI) are also widely used to control particle growth and

endow the nanocrystals with solubility and surface functionality.^{15,16} Particularly, the PEI-coated nanoparticles provide a platform for direct surface functionalization of biomolecules by bioconjugate chemistry.¹⁷

The thermal decomposition method has been developed by Yan's group¹⁸ to synthesize highly monodisperse LaF₃ nanocrystals. The approach was later extended as a common route to the synthesis of high quality UC NaYF₄ nanocrystals (Fig. 4c–f).^{19,20} For example, Capobianco and co-workers²¹ have reported the synthesis of NaYF₄ nanocrystals co-doped with Yb/Er or Yb/Tm *via* the thermal decomposition of metal trifluoroacetate precursors in the presence of oleic acid and octadecene. In their studies, the non-coordinating octadecene was used as the primary solvent due to its high boiling point (315 °C). Oleic acid was chosen not only as a solvent but also as a passivating ligand that prevents the nanocrystals from agglomeration. In their most recent work, Capobianco and co-workers²⁰ further refined this technique to synthesize UC NaYF₄ nanocrystals with a remarkably narrow size distribution without the need for size-selective fractionation (Fig. 4e and f). The approach was based on temporal separation of nucleation and crystal growth by slow addition of the precursors to the solution and subsequent manipulation of the temperature.

While the thermal decomposition method has proven useful for the synthesis of monodisperse nanocrystals, multiple groups have attempted to employ hydro(solvo)thermal synthesis to generate UC nanocrystals with controlled crystal sizes and good dispersibility in solutions. The hydro(solvo)thermal synthesis utilizes a solvent under pressures and temperatures above its critical point to increase the solubility of solid and to speed up reaction between solids. Possible advantages of this method over other types of synthetic methods include the ability to create highly crystalline phases at much lower temperatures. Disadvantages of the method include the need for specialized reaction vessels known as autoclaves and the impossibility of observing the nanocrystal as it grows. The autoclaves usually consist of

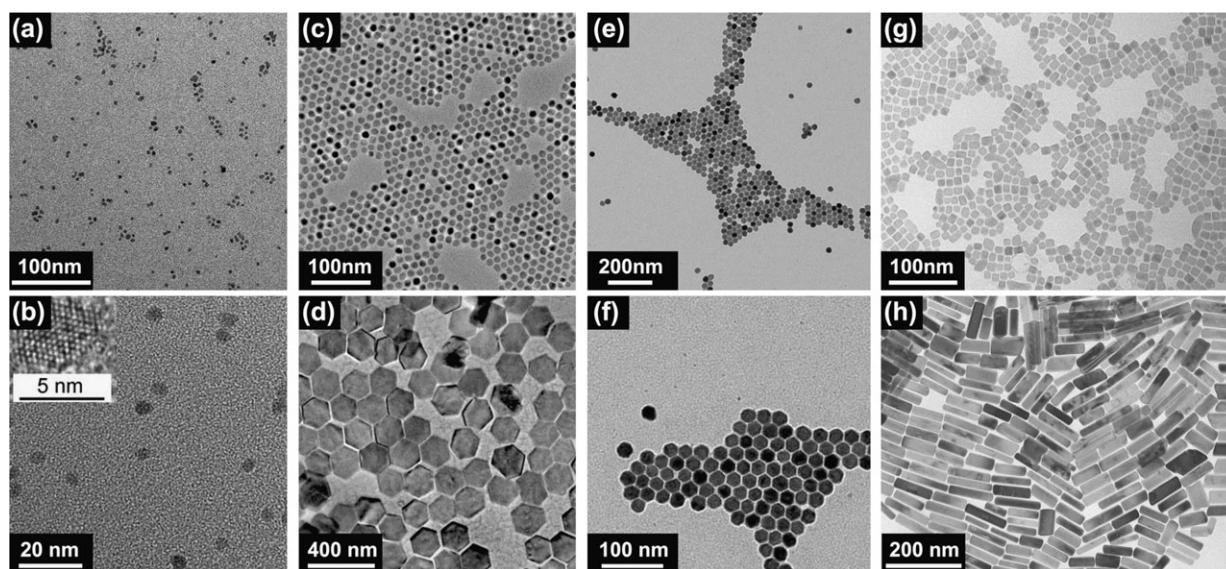


Fig. 4 TEM images of UC nanocrystals from refs. 11, 19, 20, and 23. (a), (b) (ref. 11) $\text{LaF}_3\text{:Yb/Er}$ nanoparticles prepared by Chow and co-workers. (c), (d) (ref. 19) $\text{NaYF}_4\text{:Yb/Er}$ nanoparticles and nanoplates prepared by Yan and co-workers. (e), (f) (ref. 20) Monodisperse $\text{NaYF}_4\text{:Yb/Er}$ nanoparticles prepared by Capobianco and co-workers. (g), (h) (ref. 23) $\text{NaYF}_4\text{:Yb/Er}$ nanoparticles and nanorods prepared by Li and co-workers. (Reprinted with permission. Copyright 2005, 2006, 2007, Royal Society of Chemistry and American Chemical Society)

thick-walled steel cylinders with a hermetic seal for carrying out chemical reactions under pressure and high temperatures for prolonged periods of time. Furthermore, protective contact-type inserts typically made of Teflon and titanium materials are generally required to prevent solvent corrosion of the internal cavity of the autoclave. Polyol- or micelle-mediated solvothermal methods have also been utilized for the synthesis of UC nanocrystals with tunable crystal size and morphology (Fig. 4g and h).^{22,23} Another interesting development was reported by Zhao and co-workers,²⁴ who utilized an oleic acid-mediated hydrothermal method for the synthesis of UC NaYF_4 nanorods, nanotubes, and flower-patterned nanodisks (Fig. 5). Recently, $\text{LaF}_3\text{:Yb/Er(Tm,Ho)}$ nanoplates with multicolor UC fluorescence were synthesized *via* a hybrid thermal decomposition/solvothermal method.²⁵

Sol-gel processing is a typical wet-chemical technique for the fabrication of UC nanocrystals for applications as thin film coating and glass materials. The sol-gel process is characterized by the hydrolysis and polycondensation of metal alkoxide (or halide) based precursors. To improve the crystallinity that is directly associated with luminescence efficiency of the nanocrystals, calcination at high temperatures is often needed. Prasad *et al.*²⁶ developed an interesting variation of the sol-gel method that produces Er^{3+} -doped ZrO_2 nanocrystals. The method involves a sol-emulsion-gel technique that utilizes reverse micelles formed in emulsions as the reactors for growing nanocrystals. The sol-gel process was also developed for a variety of UC nanocrystals with metal oxides as host materials including $\text{TiO}_2\text{:Er}$, $\text{BaTiO}_3\text{:Er}$, $\text{Lu}_3\text{Ga}_5\text{O}_{12}\text{:Er}$, and $\text{YVO}_4\text{:Yb/Er}$.^{27–29} Despite extensive research efforts in this area, the sol-gel derived nanocrystals are not particularly suitable as luminescent probes for biological assays due to lack of particle size control and considerable aggregation of the particles when dispersed in aqueous solutions.

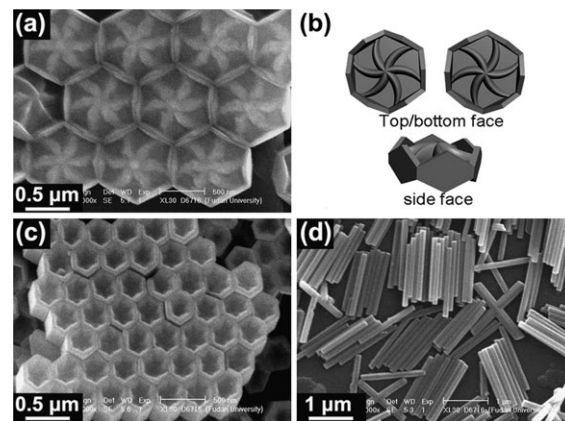


Fig. 5 (a) SEM image of arrays of flower-patterned hexagonal disks of $\beta\text{-NaYF}_4$. (b) The top- and side-view SEM images of the disk. (c), (d) SEM images of arrays of $\beta\text{-NaYF}_4$ hexagonal nanotube and nanorods, respectively. (Reprinted with permission from ref. 24. Copyright 2007, Wiley-VCH Verlag GmbH & Co. KGaA)

In stark contrast to sol-gel and hydro(solvo)thermal methods that often require heating for a prolonged time period up to several days at high temperatures to complete a synthesis, controlled explosions in reactions known as combustion synthesis can give reaction products in minutes. Once initiated by a heat source, highly exothermic reactions with temperatures ranging typically from 500 to 3000 °C occur in the form of a combustion wave that propagates through the reaction materials in a self-sustained manner without requiring additional heat. The energy saving method represents one of the attractive techniques to synthesize a wide variety of oxide and oxysulfide UC nanocrystals (Y_2O_3 , $\text{La}_2\text{O}_2\text{S}$, and Gd_2O_3) reported by the groups of Capobianco, Luo, and Zhang.^{30–32}

Flame synthesis is another time-saving technique for the synthesis of UC nanocrystals in a single-step process. In addition, flame synthesis is a continuous and readily scalable method with potential for considerably lower cost UC nanocrystal production than is available from other methods. Recently, Ju and co-workers³³ reported the synthesis of $Y_2O_3:Yb/Er(Tm, Ho)$ nanocrystals using the flame synthesis method. Their results also showed that particle size, morphology, and photoluminescence intensity are strongly affected by flame temperature.

4. Surface modification

Surface modification of lanthanide-doped nanocrystals not only improves photostability of the nanocrystals with desirable interfacial properties, but also provides a potential platform for attaching biological macromolecules for various biomedical applications.

4.1 Surface passivation

Lanthanide-doped nanocrystals normally have a high proportion of surface dopant ions in incomplete coordination environments. Luminescence of the surface dopant ions is readily quenched by high energy oscillators arising from weakly bound surface impurities, ligands, and solvents due to lack of effective protection by the host lattice. Excitation energy of the interior ions can also be transferred to the surface through adjacent dopant ions and eventually dissipated non-radiatively. In addition, incomplete coordination environments result in a decrease of the crystal-field strength around the surface dopant ions and consequently lead to low efficiency of UC luminescence. Therefore, it is generally believed that UC emission of nanocrystals is more inefficient than that of their corresponding bulk materials.

The introduction of an inert crystalline shell of an undoped material around each doped nanocrystal provides an effective way to improve the UC efficiency of lanthanide-doped nanocrystals (Fig. 6). The shell usually has the same composition as the nanocrystal host. In such structures, all dopant ions are confined in the interior core of the nanocrystals, effectively

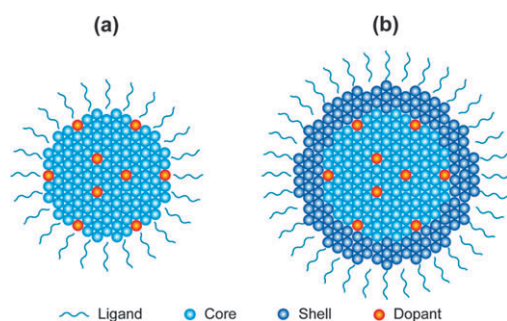


Fig. 6 Proposed statistical distributions of lanthanide dopants in (a) a nanocrystal without the protection of a shell and (b) a core-shell type nanocrystal. The non-protected nanocrystal features a relatively large number of surface dopant ions that are poorly luminescent. In contrast, all dopant ions in the core-shell nanocrystal are confined in the interior core of the crystal and participate in efficient luminescence.

suppressing energy transfer to the crystal surface to result in efficient UC luminescence. An excellent demonstration was made by Chow *et al.*³⁴ who recently reported a luminescence enhancement of nearly 30 times for 8 nm $NaYF_4:Yb/Tm$ nanocrystals coated with a 1.5 nm thick $NaYF_4$ shell. Yan *et al.*³⁵ also have reported a two-fold increase in luminescence intensity of $NaYF_4:Yb/Er$ nanocrystals after the growth at the surface of a crystalline $NaYF_4$ shell.

Amorphous shells also have been used to minimize surface quenching effects and improve the luminescence efficiency of UC nanocrystals. Lü and co-workers³⁶ have reported the preparation of $Y_2O_3:Yb/Tm$ nanocrystals that were coated with non-crystalline silica or titania shells. The UC luminescence intensities of the nanocrystals can be varied by adjusting the thickness of the amorphous shells. Although this approach provides photoemission intensity tunability in nanocrystals, the luminescence yields of the nanocrystals are limited due to the weak ligand fields and high energy oscillations from the non-crystalline silica shells. Further improvement of luminescence properties of the nanocrystals can be expected through the controlled growth of a crystalline inner shell and a silica outer shell.

4.2 Surface functionalization

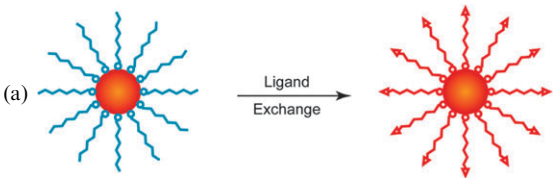
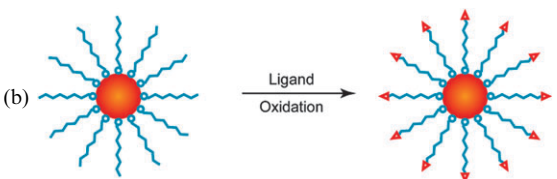
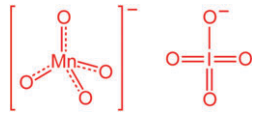
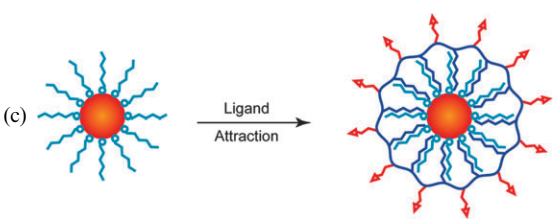
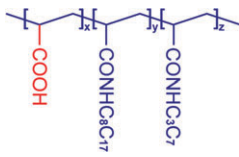
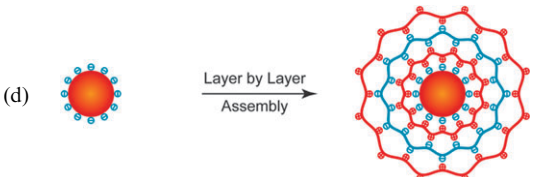
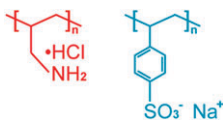
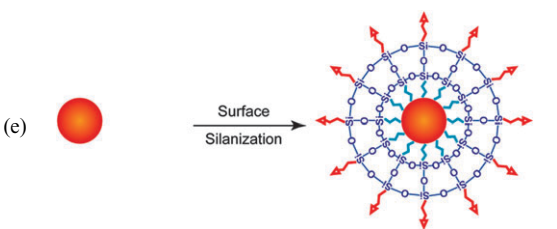
For biological labeling applications, a lanthanide-doped nanocrystal should not only exhibit high UC luminescence efficiency, but also have surface wetting characteristics that are compatible with biomolecules or biomolecular assemblies such as live cells. Most of the UC nanocrystals prepared using high-temperature routes described above have no intrinsic aqueous solubility and lack functional moieties. Surface functionalization with hydrophilic ligands is required prior to chemical attachment of biomolecules. Table 2 lists representative strategies that are currently being investigated by several different groups to provide UC nanocrystals with dual surface properties (solubility and functionality) for biomedical applications and biodetection schemes.

Chow and co-workers³⁷ have reported the ligand exchange preparation of water-soluble $NaYF_4:Yb/Er$ nanoparticles that were previously stabilized with oleylamine ligands (Table 2a). This technique utilized bifunctional organic molecules (polyethylene glycol 600 diacid) that replace the amine ligand to provide a water-soluble carboxyl-functionalized surface, which is also capable of immobilization to biological assemblies *via* bioconjugate chemistry.

Alternatively, surface functionalization can be achieved by a ligand oxidation technique. Li *et al.*³⁸ have demonstrated conversion of oleic acid-stabilized hydrophobic $NaYF_4:Yb/Er$ nanoparticles into water-dispersible nanoparticles with Lemieux-von Rudloff reagent (Table 2b). The oxidation process transforms monounsaturated carbon-carbon double bonds into carboxylic acid groups that provide reactive functional moieties for subsequent biofunctionalization. One drawback of this method is that it is only applicable to a limited number of ligands containing unsaturated carbon-carbon bonds.

In both cases discussed above, the methods for forming hydrophilic nanocrystals from hydrophobic counterparts

Table 2 Generic strategies for solubilization and functionalization of UC nanocrystals

Schematic of strategies	Representative reagents	Remarks
		<p>Ligand Exchange involves displacement of original ligands by bifunctional polymeric molecules. The polymer, when applied to a nanocrystal substrate, can provide a hydrophilic surface and additional bioconjugation capability.</p>
		<p>Ligand Oxidation involves oxidation of the carbon-carbon double bond of the ligand by Lemieux-von Rudloff reagent to generate a pendant carboxylic functional group. This strategy is only applicable to a specific class of ligands.</p>
		<p>Ligand Attraction involves absorption of an additional amphiphilic block copolymer onto the nanocrystal surface through the hydrophobic attraction between the original ligand and hydrocarbon chain of the polymer. The hydrophilic outer block of the polymer permits aqueous dispersion and further bioconjugation.</p>
		<p>Layer by Layer Assembly involves electrostatic adsorption of alternately charged polyions on the nanocrystal surface. The layer thickness of the polyions can be precisely controlled. This strategy is only applicable to hydrophilic nanocrystals.</p>
		<p>Surface Silanization involves growing an amorphous silica shell on the nanocrystal core by hydrolysis and condensation of siloxane monomers. Silanes having diverse functional groups impart rigidity to the nanocrystal and provide desirable interfacial properties such as wetting and adhesion.</p>

require ligand exchange or chemical conversion of pre-modified ligands. However, the original hydrophobic ligands on the surface of nanocrystals can be retained with the assistance of subsequent surface functionalization *via* hydrophobic van der Waals interactions with amphiphilic polymers. Using this technique, Chow and co-workers³⁴ have reported the coating of core-shell nanoparticles of NaYF₄:Yb/Er with carboxyl groups. Commercially available polyacrylic acid (PAA) was modified with 25% octylamine and 40% isopropylamine and used as the coating material (Table 2c). The hydrophilic outer block of the polymer permits aqueous dispersion and further surface derivatization.

Instead of using amphiphilic block polymers for the coupling of UC particles, Li *et al.*³⁹ have developed a

layer-by-layer (LBL) assembly strategy that uses oppositely-charged linear polyions to generate water-soluble UC nanoparticles (Table 2d). Upon sequential adsorption of positively charged poly(allylamine hydrochloride) (PAH) and negatively charged poly(sodium 4-styrenesulfonate) (PSS) onto the surface of nanoparticles, they successfully modified NaYF₄:Yb/Er nanoparticles with stable amino-rich shells. The LBL assembly technique offers many advantages, albeit requiring repeated wash steps after each adsorption step, and these include simplicity, universality, and thickness control in nanoscale. More importantly, the high stability and biocompatibility of these polyions make them attractive as coating materials for a wide range of fundamental and technological applications.

In contrast to the non-covalent electrostatic approach described above, van Veggel and co-workers⁴⁰ have prepared UC nanoparticles with covalently attached polymers *via* a surface silanization technique. In their study, organosilanes with pendant amine functional groups are assembled onto the surface of lanthanide-doped LaF₃ nanoparticles to form a thin layer of silica (Table 2e). Covalent attachment of the modified nanoparticles to biotin-*N*-hydroxysuccinimide activated esters produces stable luminescent biolabels. By using an approach analogous to the aforementioned method, Zhang *et al.*¹⁵ have reported the silica coating of PVP-stabilized NaYF₄:Yb/Er nanoparticles in a mixture of ethanol–water solutions. The thickness of the coated silica layer can be precisely adjusted from 10 nm to 1 nm by controlling the concentration of tetraethoxysilane (TEOS), a precursor for silica formation by hydrolysis and polycondensation. The silica-coated NaYF₄:Yb/Er nanoparticles are photostable, monodisperse, and can be readily dispersed in aqueous solvents.

It is important to note that the surface silanization technique is applicable for both hydrophilic and hydrophobic UC nanocrystals. The coating process of hydrophilic nanocrystals relies on the well-known Stöber method described above, while the coating process of hydrophobic nanocrystals typically utilizes a reverse-microemulsion method (Fig. 7).^{41,42} One intriguing approach for fabricating silica-coated magnetic UC nanoparticles was recently developed by Xue and co-workers.⁴² By using a reverse-microemulsion technique, they were able to fabricate bifunctional silica nanoparticles containing magnetic cores of iron oxide and luminescent

NaYF₄:Yb/Er nanocrystals (Fig. 7c and d). The combination of UC luminescence and magnetism should offer a powerful tool, allowing manipulation of the nanoparticles by magnetic fields and real-time visualization/detection by fluorescence imaging techniques.

5. Upconversion multicolor tuning

The ability to manipulate UC color output of lanthanide-doped nanocrystals is particularly important for their applications in multiplexed biological labeling. Ideal nanocrystal labels for multiplexed labeling would require considerable photochemical stability, strong absorption at a given excitation wavelength, and well-resolved emission spectra with narrow bandwidths. To meet these requirements, several complementary strategies have been developed to provide multiple, individually addressable emission colors.

5.1 Controlling dopant–host combination

Utilization of varied dopant–host combinations is the most straightforward approach to the generation of multicolor UC nanocrystals. Each lanthanide ion has a unique set of energy levels and generally exhibits a set of sharp emission peaks with distinguishable spectroscopic fingerprints. The luminescence from a given lanthanide ion in different host materials may vary considerably due to the different site symmetries of the dopant ions in the various host crystals. By adjusting different combinations of dopant ions and host materials, the emission wavelength and relative intensity of emission peaks can be effectively controlled to modulate emission colors of the lanthanide-doped nanocrystals.

Table 3 lists the typical dopant–host combinations used in the literature to prepare multicolor UC nanocrystals. All these systems contain Yb³⁺ ions, which are either intentionally added or act as host lattice constituents, to absorb excitation radiation. The first demonstration of efficient multicolor UC emission in solutions of lanthanide-doped nanocrystals was reported by Haase and co-workers.⁹ As shown in Fig. 8, the Yb/Er and Yb/Tm co-doped NaYF₄ nanoparticles show strong yellow (Fig. 8a) and blue (Fig. 8d) emissions, respectively. The yellow color of Er³⁺ ions results from two major constituent emissions, which can be separately observed with the aid of green and red color filters, respectively (Fig. 8b and c). Recently, Nann *et al.*⁴³ have demonstrated four-color emissions from NaYbF₄:Tm, NaYbF₄:Ho, NaYbF₄:Er, and NaYF₄:Yb nanocrystals, respectively. Under a single wavelength excitation at 980 nm, the nanoparticle solutions exhibit characteristic emission spectra and four different colors without the use of any color filter (Fig. 9). The results of this work are important considering it is the first demonstration of four-color multiplexing by using UC nanocrystals.

Although different dopant–host combinations can lead to multiple UC emissions, the color output that can be produced by this method is somewhat limited and associated with several apparent drawbacks. Nanoparticles in the form of different host materials can exhibit significantly different surface chemistry, while nanoparticles with different dopant ions generate only a limited number of efficient UC colors upon activation with Tm³⁺, Er³⁺, and Ho³⁺ ions.

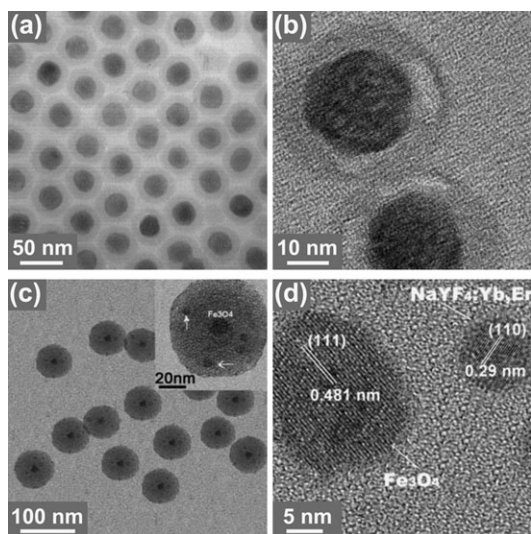


Fig. 7 TEM images from refs. 41 and 42 of silica-coated UC nanocrystals prepared by reverse-microemulsion method. (a), (b) (ref. 41) Monodisperse SiO₂-coated NaYF₄:Yb/Er nanoparticles. (c), (d) (ref. 42) TEM and HRTEM images of silica nanoparticles encapsulating UC NaYF₄:Yb/Er nanocrystals and superparamagnetic (SPM) Fe₃O₄ nanocrystals. The inset in (c) is the higher magnification image showing the simultaneous presence of both SPM nanocrystals (larger crystallites) and UC nanocrystals (finer crystallites denoted by arrows) within one single SiO₂ particle. (Reprinted with permission. Copyright 2008, Elsevier B.V. and Royal Society of Chemistry)

Table 3 Typical dopant–host combinations for making multicolored UC nanocrystals

Dopant Yb ³⁺ +	Host	Major emissions ^a (nm)			Ref.
		Blue	Green	Red	
Tm ³⁺	α -NaYF ₄	450,475 (S)		647 (W)	9
	β -NaYF ₄	450,475 (S)			37
	LaF ₃	475 (S)			25
	LuPO ₄	475 (S)		649 (S)	12
Er ³⁺	α -NaYF ₄	411 (W)	540 (M)	660 (S)	9
	β -NaYF ₄		523,542 (S)	656 (M)	37
	LaF ₃		520,545 (S)	659 (S)	25
	YbPO ₄		526,550 (S)	657,667 (S)	12
	Y ₂ O ₃		524,549 (W)	663,673 (S)	33
	α -NaYbF ₄		540 (S)		43
Ho ³⁺	LaF ₃		542 (S)	645,658 (M)	25
	Y ₂ O ₃		543 (S)	665 (M)	33

^a S, M and W refer to strong, moderate and weak emission intensities, respectively.

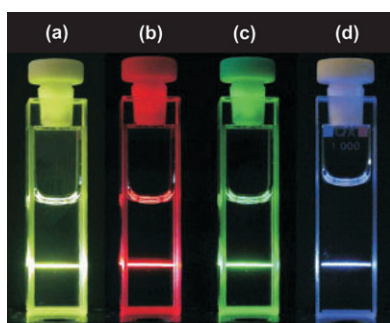


Fig. 8 Photographs of the UC luminescence in 1 wt% colloidal solutions of nanocrystals in dimethyl sulfoxide (DMSO) excited at 10270 cm⁻¹. (a) Total UC luminescence of the NaYF₄:Yb/Er (20/2 mol%) sample. (b), (c) show the same luminescence through red and green color filters, respectively. (d) Total UC luminescence of the NaYF₄:Yb/Tm (20/2 mol%) sample. (Reprinted with permission from ref. 9. Copyright 2004, Wiley-VCH Verlag GmbH & Co. KGaA)

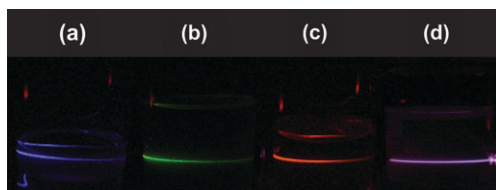


Fig. 9 UC luminescence pictures of (a) NaYbF₄:Tm, (b) NaYbF₄:Ho, (c) NaYbF₄:Er, and (d) NaYF₄:Yb nanocrystals in chloroformic solutions. These pictures were taken without the use of any color filter. (Reprinted with permission from ref. 43. Copyright 2008, American Chemical Society)

5.2 Controlling nanocrystal size

The UC emission color of lanthanide-doped nanocrystals can be modified by changes in the size of the nanocrystals. Several groups have examined the size-dependent solid-state optical properties of the lanthanide-doped nanocrystals. Most notable of these studies has been the observation by Capobianco *et al.*³⁰ of red emission enhancement in 20-nm Y₂O₃:Yb/Er nanoparticles relative to their corresponding bulk materials. In addition, Song and co-workers⁴⁴ have recently examined Y₂O₃:Yb/Er nanoparticles with different sizes (13–55 nm) and

observed that the relative emission intensity of blue to green also can be tuned with decreasing particle size.

It is important to note that this size-dependent optical property results from surface effects rather than quantum confinement effects due to the small Bohr radius of the exciton in the lanthanide-doped nanocrystals. As the nanocrystals grow smaller, the concentration of surface dopant ions is steadily increased. The emission spectrum of the nanocrystals is a sum of emissions from dopant ions at the surface and in the interior of the particles. By controlling the size of the nanocrystals, the concentration of surface dopant ions can be precisely modulated, leading to a gradual variation in emission color.

Recently, Yan *et al.*³⁵ have reported the size-dependent UC emission of α -NaYF₄:Yb/Er nanoparticles dispersed in solutions. The emission spectra of the 5.1 nm and 8 nm nanoparticles are dominated by the red (⁴F_{9/2} → ⁴I_{15/2}) and green (²H_{11/2}, ⁴S_{3/2} → ⁴I_{15/2}) color emissions, respectively. One drawback of this method is that it requires the preparation of relatively small particles (typically less than 10 nm) and without protection of an inert shell. Within this size range, the surface dopant ions become prevalent and dominate the contribution over the interior dopant ions to color emission modulation.

5.3 Controlling dopant concentration

The UC emission color also varies with the concentration of the dopant ions. The dopant concentration, which determines relative amount of the dopant ions in the nanocrystals as well as the average distance between neighboring dopant ions, has a strong influence on the optical properties of the nanocrystals. For example, an increase in the dopant concentration of Yb³⁺ in Y₂O₃:Yb/Er nanoparticles induces enhanced back-energy-transfer from Er³⁺ to Yb³⁺, thereby leading to a relative increase in intensity of red emission of Er³⁺.³⁰ A similar phenomenon also has been observed by Zhang *et al.*⁴⁵ in ZrO₂ nanocrystals co-doped with Yb/Er. By reducing the concentrations of both Yb³⁺ and Er³⁺ ions, Li and co-workers³⁹ have observed a relative decrease in intensity of red emission in NaYF₄:Yb/Er nanocrystals.

Recently, a general and versatile approach¹⁷ was developed in our lab to fine-tune the UC emission in a broad range of

color output by single wavelength excitation at 980 nm. The approach is based upon a single host source of α -NaYF₄ doped with varied amounts of Yb³⁺, Tm³⁺, and Er³⁺ ions (Fig. 10). Upon excitation at 980 nm, the NaYF₄ nanoparticles co-doped with Yb/Er (18/2 mol%) exhibit sharp emission peaks, which can be attributed to ²H_{9/2} → ⁴I_{15/2}, ²H_{11/2}, ⁴S_{3/2} → ⁴I_{15/2}, and ⁴F_{9/2} → ⁴I_{15/2} transitions of Er³⁺ (Fig. 10a). These peaks correspond to respective blue, green, and red emissions that result in an overall yellow color output (Fig. 10k). Importantly, introduction of an elevated amount of Yb³⁺ dopants in the NaYF₄ host lattice would decrease Yb··Er inter-atomic distance and thus facilitate back-energy-transfer from Er³⁺ to Yb³⁺. The energy transfer should subsequently suppress the population in excited levels of ²H_{9/2}, ²H_{11/2} and ⁴S_{3/2}, resulting in the decrease of blue (²H_{9/2} → ⁴I_{15/2}) and green (²H_{11/2}, ⁴S_{3/2} → ⁴I_{15/2}) light emissions (Fig. 10c). By precisely manipulating the relative emission intensities of the three constituent colors with increased concentrations of Yb³⁺ (25–60 mol%), we were able to control color output of the nanoparticles from yellow to red (Fig 10l–n).

We also have demonstrated that UC multicolor fine-tuning in the visible spectral region can be alternatively achieved *via* a three-component dopant system (NaYF₄:Yb/Er/Tm) in a dual emission process. By adding two emitters (Tm³⁺ and Er³⁺) with different concentration ratios, the relative intensity of the dual emissions can be precisely controlled (Fig. 10d), resulting in tunable color output from blue to white (Fig. 10f–j). In

addition, the approach was also utilized to expand the emission fine-tuning in the NIR spectral region. By increasing the concentration of Tm³⁺ ions in the NaYF₄:Yb/Tm nanocrystals, the NIR emission of Tm³⁺ can be considerably enhanced with respect to the blue emission. The phenomenon is primarily attributed to enhanced population of the ³H₄ level generated by the energy resonant between ¹G₄ → ³H₄ and ³F₂ ← ³F₄ at elevated dopant concentration of Tm³⁺. Given the broad range of available dopant–host combinations, this approach as well as its complementary version of down-conversion multicolor tuning⁴⁶ should allow generation of a large library of emission spectra in the visible and NIR spectral region that are particularly useful in multiplexed labeling.

6. Biological applications

Zijlmans and co-workers⁴⁷ were the first to exploit lanthanide-doped phosphors' upconverting properties to study biological recognition events. Since then, there has been a substantial contribution to the development of biological labeling strategies that rely on the use of UC nanocrystals. Although early in their development, these strategies have been shown to be particularly attractive in biological assays and biomedical imaging. Most strategies developed in recent years can be divided into three categories: *in vitro* detection, *in vivo* imaging, and molecular sensing *via* fluorescence resonance energy transfer (FRET).

6.1 *In vitro* detection

UC nanocrystals have been used as luminescent reporters in a variety of *in vitro* assays, including immunoassay, bioaffinity assay, and DNA hybridization assay, which offer dramatically enhanced signal-to-noise ratio and thus improved detection limits compared to conventional reporters. For example, Hampl *et al.*⁴⁸ have reported a detection limit of 10 pg human chorionic gonadotropin in a 100- μ l sample by using submicron-sized Y₂O₃:Yb/Er particles in immunochromatographic assays. A 10-fold improvement over conventional labeling systems such as colloidal gold or colored latex beads was achieved. In a parallel development, Tanke *et al.*⁴⁹ have reported a detection limit of 1 ng μ l⁻¹ probe DNA by using 400-nm Y₂O₃:Yb/Er particles, which is a four-fold increase in sensitivity compared to the detection by using cyanine 5 (Cy5) labels (Fig. 11).

Simultaneous detection of multiple analytes using multi-color UC nanocrystals has also been demonstrated by Niedbala and co-workers.⁵⁰ In a lateral flow based competitive inhibition assay, a selection of drugs containing low concentrations of amphetamine, methamphetamine, phencyclidine (PCP), and opiates were detected in a single multiplexed assay strip. To achieve the multiplexed detection, antibodies for PCP and amphetamine were conjugated to green-emitting particles while methamphetamine and morphine were conjugated to blue-emitting particles. The antibody-modified particles were then applied to the strip labeled with haptent–BSA conjugate. The detection format presented in their study should be readily applicable for the multiplexed detection of a broad range of biological systems in a single test.

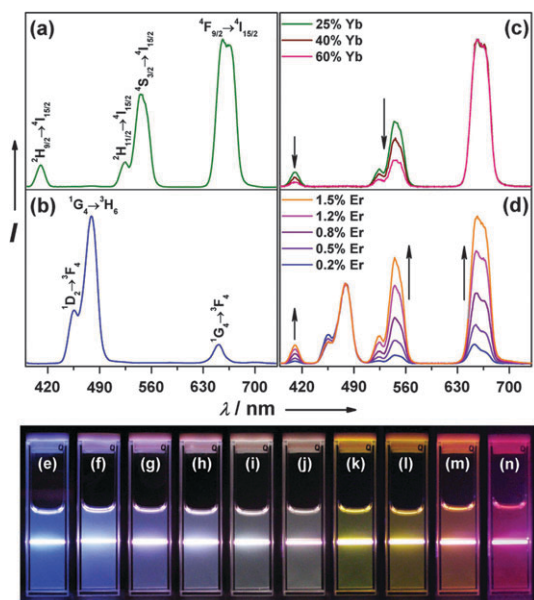


Fig. 10 Room temperature UC emission spectra of (a) NaYF₄:Yb/Er (18/2 mol%), (b) NaYF₄:Yb/Tm (20/0.2 mol%), (c) NaYF₄:Yb/Er (25–60/2 mol%), and (d) NaYF₄:Yb/Tm/Er (20/0.2/0.2–1.5 mol%) particles in ethanol solutions (10 mM). The spectra in (c) and (d) were normalized to Er³⁺ 660 nm and Tm³⁺ 480 nm emissions, respectively. Compiled luminescent photos showing corresponding colloidal solutions of (e) NaYF₄:Yb/Tm (20/0.2 mol%), (f–j) NaYF₄:Yb/Tm/Er (20/0.2/0.2–1.5 mol%), and (k–n) NaYF₄:Yb/Er (18–60/2 mol%). (Reprinted with permission from ref. 17. Copyright 2008, American Chemical Society)

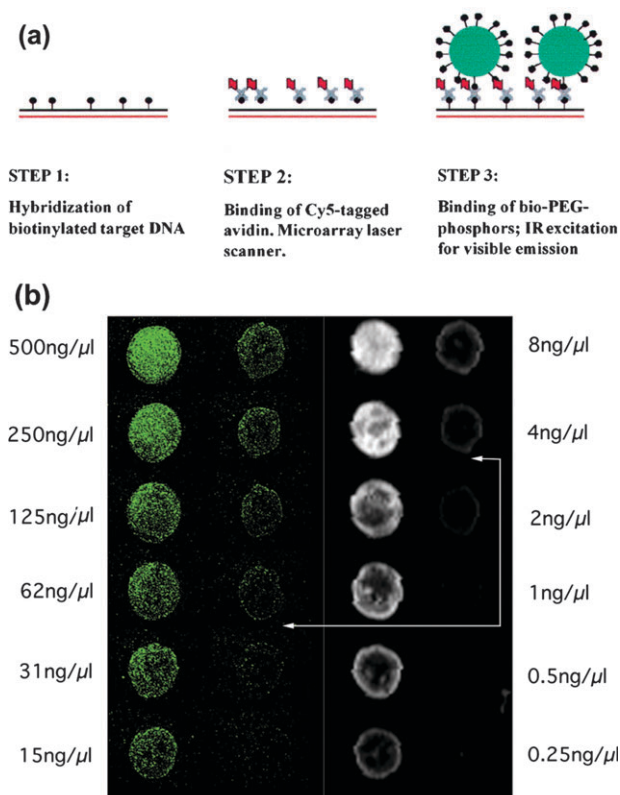


Fig. 11 (a) Schematic representation of the experiment designed to compare the detection sensitivity provided by conventional Cy5 fluorescence (microarray laser scanner) and UC phosphor particles (two-photon IR wide-field excitation for visible fluorescence). (b) Model low-complexity microarray hybridization with biotin human elongation factor (HEF)-DNA detected with avidin-Cy5 and laser scanning (right panel) and subsequent detection with biotin-polyethylene glycol (Bio-PEG) UC phosphor (left panel). Concentrations of HEF probe DNA solutions used for spotting are given next to the spots ($500\text{--}0.25\text{ ng }\mu\text{l}^{-1}$). Concentrations along the left side refer to the first and third columns, whereas those on the right refer to the second and fourth columns. Arrows indicate detection sensitivity. (Reprinted with permission from ref. 49. Copyright 2001, Nature Publishing Group)

6.2 *In vivo* imaging

Organic fluorophores and fluorescent proteins have been traditionally used for *in vivo* imaging, but they typically suffer from low photostability and strong background autofluorescence in the visible spectrum. Their broad emission bands often result in significant spectral overlapping, which can be a problem in spectral interpretation during multicolor imaging. Quantum dots are more photostable than the organic fluorophores and have relatively narrow emission bandwidths. Their potential cytotoxicity over time, however, remains to be established. In contrast, lanthanide-doped UC nanocrystals generally contain less toxic elements. With their photostable fluorescence and minimized background autofluorescence by NIR excitation, the lanthanide-doped nanocrystals show great promise as alternatives to organic fluorophores and quantum dots for *in vivo* bioimaging.

Lim *et al.*⁵¹ have demonstrated that $\text{Y}_2\text{O}_3\text{:Yb/Er}$ nanoparticles in the size range of 50–150 nm can be inoculated

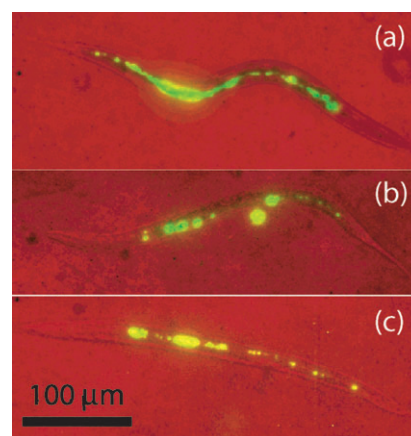


Fig. 12 False color two-photon images of *C. elegans* at 980-nm excitation with red representing the bright field and green for the phosphor emission. The worms were deprived of food over a period of 24 h, showing little or no change at (a) 0 h, (b) 4 h, and (c) 24 h. (Reprinted with permission from ref. 51. Copyright 2006, American Chemical Society)

into live nematode *C. elegans* and imaged in the digestive system of the worms. Upon excitation at 980 nm, the statistical distribution of the nanoparticles in the intestines can be clearly visualized (Fig. 12). Importantly, the nanoparticles have shown good biocompatibility as the worms do not exhibit notable defects in feeding.

An intriguing recent development was demonstrated by Zhang and co-workers⁵² for *in vivo* imaging in anesthetized Wistar rats by using 50-nm $\text{NaYF}_4\text{:Yb/Er}$ nanoparticles

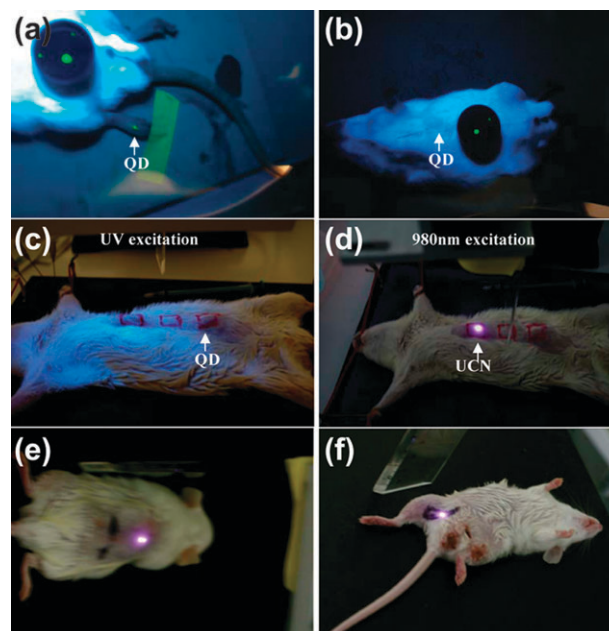


Fig. 13 *In vivo* imaging of rat injected with quantum dots shows fluorescence through (a) the translucent skin of the foot and, but not through (b) the thicker back skin or (c) abdomen. $\text{NaYF}_4\text{:Yb/Er}$ nanoparticles injected below (d) abdominal skin, (e) thigh muscles, or (f) back skin show luminescence. Quantum dots on a black disk in (a, b) are used as the control. (Reprinted with permission from ref. 52. Copyright 2008, Elsevier B.V.)

(Fig. 13). The rats were injected with the nanoparticles under the skin in the groin and upper leg regions. Using a combination of simple optical techniques and a 980-nm NIR laser, the nanoparticles can be detected up to 10 mm beneath the skin, far deeper than depths managed through use of quantum dots. This method holds promise for providing a new technique for imaging tissue structures at different depths and for performing minimally invasive detection.

6.3 FRET-based sensing

UC nanocrystals have been coupled with metallic nanoparticles or organic fluorophores for FRET-based biomolecular detection (Fig. 14). By using biotinylated NaYF₄:Yb/Er nanoparticles as energy donors and biotinylated gold nanoparticles as energy acceptors, Li *et al.*³⁹ have developed a highly sensitive biosensor for detection of avidin. The 7-nm gold nanoparticles show a broad and strong absorption centered at 520 nm, which matches well with the 540-nm emission of NaYF₄:Yb/Er nanoparticles. Addition of the avidin to the sensor system triggers aggregation of gold and UC nanoparticles because of the specific interaction between the avidin and biotin, thus bringing the donor and acceptor into close proximity. Consequently, the emission intensity of the UC nanoparticles decreases when energy transfer occurs from the donor to acceptor. This method registers an unoptimized detection limit of 0.5 nM.

Recently, Zhang *et al.*⁵³ adopted an alternative mode of FRET-based biomolecule detection. Instead of using metallic nanoparticles, they utilized an organic dye as an energy acceptor or quencher for donor–acceptor energy transfer. With the organic dye, they demonstrated a detection limit of 1.3 nM for a 26-base oligonucleotide. They also showed that single-base mismatch detection using oligonucleotide-modified

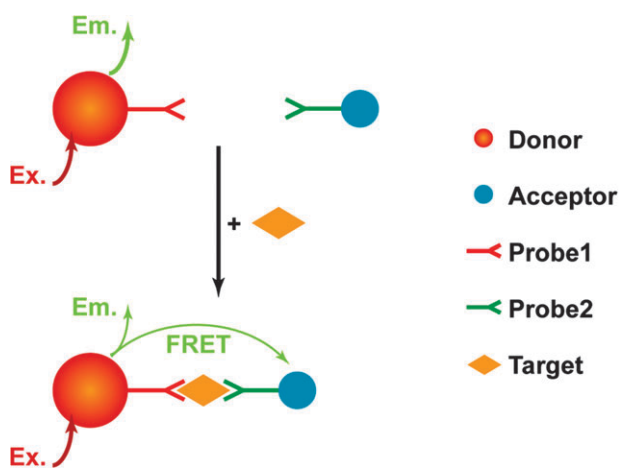


Fig. 14 Schematic of a FRET-based sensor system. The system involves the use of UC nanocrystals as energy donors and other optical materials as energy acceptors. The donor and acceptor are modified with molecular probes that can specifically bind to a target. When the target is absent, the donor and acceptor are well separated and no FRET process is expected. In the presence of the target, however, the donor and acceptor will be linked in close proximity and FRET becomes significant, resulting in a decrease in emission intensity of the donor. Note that sensitized emission from the acceptor can also be expected.

UC nanoparticles could be achieved. One drawback of this application is the short range of the FRET process, which requires stringent control over the surface modification of the UC nanoparticles. The thickness of the coating layer must be minimized to ensure a proximal contact between the UC nanoparticle and fluorophore for efficient energy transfer.

7. Conclusions

This review has described the recent development of lanthanide-doped UC nanocrystals with emphasis on synthetic strategies, surface modification, multicolor emission tuning, and biological applications. This research continues to be a vibrant and growing interdisciplinary field. The number of available dopant–host compositions is increasing, and new opportunities for these complex optical materials are arising. Despite the gains, many significant challenges certainly remain before their full potential can be realized for practical applications in clinical and point-of-care settings. One weak link is the lack of a generalized protocol for the controlled synthesis and surface modification of UC nanocrystals that exhibit high colloidal stability and tailorable optical properties. Substantial efforts are also needed to focus on development of strategies for patterning UC nanocrystals on various substrates, allowing for multiplexed high-sensitivity detection and integration with miniaturized electronic devices on a low-cost, high-throughput platform.

Acknowledgements

X.L. acknowledges the National University of Singapore (NUS), the Defence Science & Technology Agency (DSTA), the Singapore-MIT Alliance (SMA), and the Agency for Science, Technology and Research (A*STAR) for supporting this work. X.L. is grateful to the NUS for a Young Investigator Award.

References

- 1 F. Auzel, *Chem. Rev.*, 2004, **104**, 139.
- 2 J. F. Suyver, A. Aebischer, D. Biner, P. Gerner, J. Grimm, S. Heer, K. W. Krämer, C. Reinhard and H. U. Güdel, *Opt. Mater.*, 2005, **27**, 1111.
- 3 F. Wang, W. Tan, Y. Zhang, X. Fan and M. Wang, *Nanotechnology*, 2006, **17**, R1.
- 4 K. König, *J. Microsc.*, 2000, **200**, 83.
- 5 J. S. Chivian, W. E. Case and D. D. Eden, *Appl. Phys. Lett.*, 1979, **35**, 124.
- 6 J. W. Stouwdam and F. C. J. M. van Veggel, *Nano Lett.*, 2002, **2**, 733.
- 7 J. M. F. van Dijk and M. F. H. Schuurmans, *J. Chem. Phys.*, 1983, **78**, 5317.
- 8 A. A. Bol, R. van Beek and A. Meijerink, *Chem. Mater.*, 2002, **14**, 1121.
- 9 S. Heer, K. Kömpe, H. U. Güdel and M. Haase, *Adv. Mater.*, 2004, **16**, 2102.
- 10 G. Blasse and B. C. Grabmaier, *Luminescent Materials*, Springer, Berlin, 1994.
- 11 G. Yi and G. Chow, *J. Mater. Chem.*, 2005, **15**, 4460.
- 12 S. Heer, O. Lehmann, M. Haase and H. U. Güdel, *Angew. Chem., Int. Ed.*, 2003, **42**, 3179.
- 13 G. Yi, H. Lu, S. Zhao, Y. Ge, W. Yang, D. Chen and L. Guo, *Nano Lett.*, 2004, **4**, 2191.
- 14 J. Zeng, J. Su, Z. Li, R. Yan and Y. Li, *Adv. Mater.*, 2005, **17**, 2119.
- 15 Z. Li and Y. Zhang, *Angew. Chem., Int. Ed.*, 2006, **45**, 7732.

- 16 F. Wang, D. K. Chatterjee, Z. Li, Y. Zhang, X. Fan and M. Wang, *Nanotechnology*, 2006, **17**, 5786.
- 17 F. Wang and X. Liu, *J. Am. Chem. Soc.*, 2008, **130**, 5642.
- 18 Y. Zhang, X. Sun, R. Si, L. You and C. Yan, *J. Am. Chem. Soc.*, 2005, **127**, 3260.
- 19 H. Mai, Y. Zhang, R. Si, Z. Yan, L. Sun, L. You and C. Yan, *J. Am. Chem. Soc.*, 2006, **128**, 6426.
- 20 J. C. Boyer, L. A. Cuccia and J. A. Capobianco, *Nano Lett.*, 2007, **7**, 847.
- 21 J. C. Boyer, F. Vetrone, L. A. Cuccia and J. A. Capobianco, *J. Am. Chem. Soc.*, 2006, **128**, 7444.
- 22 Y. Wei, F. Lu, X. Zhang and D. Chen, *J. Alloys Compd.*, 2008, **455**, 376.
- 23 L. Wang and Y. Li, *Chem. Mater.*, 2007, **19**, 727.
- 24 F. Zhang, Y. Wan, T. Yu, F. Zhang, Y. Shi, S. Xie, Y. Li, L. Xu, B. Tu and D. Zhao, *Angew. Chem., Int. Ed.*, 2007, **46**, 7976.
- 25 C. Liu and D. Chen, *J. Mater. Chem.*, 2007, **17**, 3875.
- 26 A. Patra, C. S. Friend, R. Kapoor and P. N. Prasad, *J. Phys. Chem. B*, 2002, **106**, 1909.
- 27 A. Patra, C. S. Friend, R. Kapoor and P. N. Prasad, *Chem. Mater.*, 2003, **15**, 3650.
- 28 V. Venkatramu, D. Falcomer, A. Speghini, M. Bettinelli and C. K. Jayasankar, *J. Lumin.*, 2008, **128**, 811.
- 29 K. Yang, F. Zheng, R. Wu, H. Li and X. Zhang, *J. Rare Earth*, 2006, **24**, 162.
- 30 F. Vetrone, J. C. Boyer, J. A. Capobianco, A. Speghini and M. Bettinelli, *J. Appl. Phys.*, 2004, **96**, 661.
- 31 X. Luo and W. Cao, *J. Alloys Compd.*, 2008, **460**, 529.
- 32 L. Xu, Y. Yu, X. Li, G. Somesfalean, Y. Zhang, H. Gao and Z. Zhang, *Opt. Mater.*, 2008, **30**, 1284.
- 33 X. Qin, T. Yokomori and Y. Ju, *Appl. Phys. Lett.*, 2007, **90**, 073104.
- 34 G. Yi and G. Chow, *Chem. Mater.*, 2007, **19**, 341.
- 35 H. Mai, Y. Zhang, L. Sun and C. Yan, *J. Phys. Chem. C*, 2007, **111**, 13721.
- 36 Q. Lü, F. Guo, L. Sun, A. Li and L. Zhao, *J. Appl. Phys.*, 2008, **103**, 123533.
- 37 G. Yi and G. Chow, *Adv. Funct. Mater.*, 2006, **16**, 2324.
- 38 Z. Chen, H. Chen, H. Hu, M. Yu, F. Li, Q. Zhang, Z. Zhou, T. Yi and C. Huang, *J. Am. Chem. Soc.*, 2008, **130**, 3023.
- 39 L. Wang, R. Yan, Z. Huo, L. Wang, J. Zeng, J. Bao, X. Wang, Q. Peng and Y. Li, *Angew. Chem., Int. Ed.*, 2005, **44**, 6054.
- 40 S. Sivakumar, P. R. Diamente and F. C. J. M. van Veggel, *Chem.–Eur. J.*, 2006, **12**, 5878.
- 41 R. A. Jalil and Y. Zhang, *Biomaterials*, 2008, **29**, 4122.
- 42 Z. Liu, G. Yi, H. Zhang, J. Ding, Y. Zhang and J. Xue, *Chem. Commun.*, 2008, 694.
- 43 O. Ehlert, R. Thomann, M. Darbandi and T. Nann, *ACS Nano*, 2008, **2**, 120.
- 44 X. Bai, H. Song, G. Pan, Y. Lei, T. Wang, X. Ren, S. Lu, B. Dong, Q. Dai and L. Fan, *J. Phys. Chem. C*, 2007, **111**, 13611.
- 45 G. Chen, Y. Zhang, G. Somesfalean, Z. Zhang, Q. Sun and F. Wang, *Appl. Phys. Lett.*, 2006, **89**, 163105.
- 46 F. Wang, X. Xue and X. Liu, *Angew. Chem., Int. Ed.*, 2008, **47**, 906.
- 47 H. J. M. A. A. Zijlmans, J. Bonnet, J. Burton, K. Kardos, T. Vail, R. S. Niedbala and H. J. Tanke, *Anal. Biochem.*, 1999, **267**, 30.
- 48 J. Hampl, M. Hall, N. A. Mufti, Y.-m. M. Yao, D. B. MacQueen, W. H. Wright and D. E. Cooper, *Anal. Biochem.*, 2001, **288**, 176.
- 49 F. van de Rijke, H. Zijlmans, S. Li, T. Vail, A. K. Raap, R. S. Niedbala and H. J. Tanke, *Nat. Biotechnol.*, 2001, **19**, 273.
- 50 R. S. Niedbala, H. Feindt, K. Kardos, T. Vail, J. Burton, B. Bielska, S. Li, D. Milunic, P. Bourdelle and R. Vallejo, *Anal. Biochem.*, 2001, **293**, 22.
- 51 S. F. Lim, R. Riehn, W. S. Ryu, N. Khanarian, C.-k. Tung, D. Tank and R. H. Austin, *Nano Lett.*, 2006, **6**, 169.
- 52 D. K. Chatterjee, A. J. Rufaihah and Y. Zhang, *Biomaterials*, 2008, **29**, 937.
- 53 P. Zhang, S. Rogelj, K. Nguyen and D. Wheeler, *J. Am. Chem. Soc.*, 2006, **128**, 12410.